A Three-Phase Current-Fed Push–Pull DC–DC Converter With Active Clamp for Fuel Cell Applications

Sangwon Lee, Junsung Park, and Sewan Choi, *Senior Member, IEEE*

***Abstract*—In this paper, a new active-clamped three-phase current-fed push–pull dc–dc converter is proposed for high-power applications where low-voltage high-current input sources such as fuel cells are used. The proposed converter has the following features: active clamping of the transient surge voltage caused by transformer leakage inductances, natural zero-voltage switching turn-on of main switches using energy stored in transformer leakage inductor, small current rating and zero-voltage and zero-current switching of clamp switches, no additional start-up circuitry for soft starting due to the operating duty cycle range between 0 and 1, and zero-current switching turn-off of rectifier diodes leading to negligible voltage surge associated with the diode reverse recovery. A comparative study along with loss analysis is performed. Experimental results from 5-kW laboratory prototypes of the proposed active-clamped converter and the passive-clamped converter [14] are provided.**

***Index Terms*—Active clamp, current-fed, fuel cells, push–pull, three-phase dc–dc converter, three-phase transformer, zero voltage switching (ZVS).**

I. Introduction

The step-up dc–dc converter with high-frequency transformer has increasingly been used in high-power applications such as fuel cell systems, photovoltaic systems, hybrid electric vehicles, and UPS where voltage step-up and galvanic isolation are required. The step-up dc–dc converter with high-frequency transformer could be either voltage-fed or current-fed type. The advantages and disadvantages of the two types are detailed in [1]. The voltage-fed converter has low switch voltage rating that is the same as input voltage, and therefore, MOSFETs with low $R_{\mathrm{ds(on)}}$ can be used, which is a significant advantage in the high step-up application where conduction losses associated with primary switches are dominant. In the high step-up application, however, the voltage-fed converter suffers from high transformer turns ratio, leading to many disadvantages associated with large leakage inductance. Compared to the voltage-fed topology, in general, the current-fed topology exhibits smaller input current ripple, lower diode voltage rating, lower transformer turns ratio, and negligible reverse recovery problem at the rectifier side [2]. Especially, lower transformer turns ratio leads to smaller duty cycle loss and transformer copper loss, which are important for efficient operation at high power levels. Direct and precise control of the input current is also possible with the current-fed topology. Therefore, the current-fed dc–dc converter is better suited to low-voltage high-current input application such as a front-end converter for fuel cell power conversion systems where high-voltage step-up ratio is required [1].

The three-phase dc–dc converter has firstly been introduced in [3]. The three-phase dc–dc converter has presented good performance in the high-power applications where high device stresses are faced when implemented with the single-phase dc–dc converter. Generally, the three-phase dc–dc converter has several advantages over its single-phase counterpart: easy MOSFETs selection due to reduced current rating, reduction of the input and output filters' volume due to increased effective switching frequency by a factor of 3, and reduction in transformer size due to better transformer utilization. There are two types of three-phase voltage-fed converters according to primary configuration: a three-phase bridge [3]–[6] and three single-phase bridges [7]. The three-phase voltage-fed converter with open $\Delta - Y$ [7] or $\Delta - Y$ [6] transformer connection can reduce the transformer turns ratio to half, which makes the voltage-converter viable for high step-up application. The converter proposed in [4] has the simplest structure, yet main switches are turned on with ZVS. The V6 converter [7] is also soft-switched and suitable for higherpower applications since it has more switch legs. The active clamp employed in [6] not only clamps surge voltage at the high-voltage secondary side but also reduces the circulating current at the high-current primary side.

The three-phase current-fed converters proposed so far can be classified by primary-side configuration into three basic topologies: full bridge [10], L-type half bridge [11]–[13], and push–pull [14]. A simple active-clamp circuit [10] was introduced into the three-phase current-fed converter in order to alleviate voltage spikes as well as achieve ZVS of switches, but switching frequency of the active-clamp switch is six times higher than that of main switches, which limits the switching frequency of the overall system. The three-phase current-fed converter based on L-type half-bridge topology was introduced in [11].

Manuscript received April 15, 2010; revised August 6, 2010 and September 28, 2010; accepted November 13, 2010. Date of current version August 10, 2011. This work has been supported by KESRI (20101020300260), which is funded by Ministry of Knowledge Economy. Recommended for publication by Associate Editor Y.-M. Chen.

S. Lee is with the Department of Research and Development Center, Changsung, Inc., Incheon 620-8, Korea (e-mail: sadyangel@paran.com).

J. Park is with Power Electronics and Fuel Cell Power Conditioning Laboratory, Seoul National University of Science and Technology, Seoul 139-743, Korea (e-mail: pjs09507@snut.ac.kr).

S. Choi is with the Department of Control and Instrumentation Engineering, Seoul National University of Science and Technology, Seoul 139-743, Korea (e-mail: schoi@snut.ac.kr).

Color versions of one or more of the figures in this paper are available online at http://ieeexplore.ieee.org.

Digital Object Identifier 10.1109/TPEL.2010.2096477

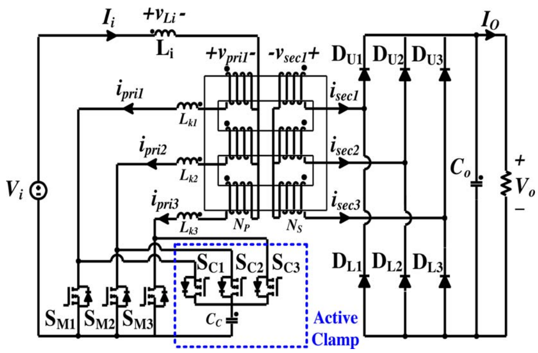

Fig. 1. Proposed three-phase push–pull dc-dc converter with active clamp.

Active-clamp circuits were applied to the three-phase L-type half-bridge converter in [12] and [13]. Besides reduced total number of switches compared to the three-phase full-bridge converter proposed in [10], a major advantage of the three-phase L-type half-bridge converter is that the switching frequency of clamp switches is the same as that of main switches, and therefore, higher power density can be achieved by further increasing the switching frequency of the overall system. A three-phase current-fed push–pull converter was introduced in [14]. The three-phase push–pull converter has the simplest structure in its power and gate drive circuits, leading to increased system reliability.

In this paper, an active-clamping technique is proposed for the three-phase current-fed push–pull converter. With the proposed active clamping, the current-fed push–pull converter is able to achieve higher efficiency and higher power density in the high step-up application such as fuel cells owing to the following features.

1) Active clamping of the transient surge voltage caused by transformer leakage inductances.
2) Natural zero voltage switching (ZVS) turn-on of main switches using energy stored in the transformer leakage inductor.
3) Small current rating and zero voltage and zero current switching (ZVZCS) of clamp switches.
4) No additional start-up circuitry required for soft starting due to the operating duty cycle range between 0 and 1.
5) Zero-current switching (ZCS) turn-off of rectifier diodes leading to negligible voltage surge associated with the diode reverse recovery.

II. Operating Principles

The circuit topology of the proposed converter is basically a three-phase, current-fed, push–pull converter with an active-clamp circuit, as shown in Fig. 1. The proposed converter includes an input filter inductor, three main switches $S_{\mathrm{M}1}$, $S_{\mathrm{M}2}$, and $S_{\mathrm{M}3}$, and a clamp circuit consisting of three clamp switches $S_{\mathrm{C}1}$, $S_{\mathrm{C}2}$, and $S_{\mathrm{C}3}$ and a clamp capacitor C_C at the low-voltage primary side, and a three-phase diode bridge at the high-voltage secondary side. Note that a three-leg core must be used for proper operation of the proposed converter. The three-phase windings are configured in *Y–Y* connection. The neutral point of the three-phase primary winding is connected to the input source through the input inductor. The proposed active-clamping method not only limits the transient-surge voltage caused by transformer leakage inductances, but also helps improve the efficiency by enabling soft switching of the main switches.

TABLE I
Operation Modes Based on the Duty Cycle

Duty cycle	No. of main switches simultaneously on	No. of clamp switches simultaneously on
$D < 0.33$	up to 1	up to 3
$0.33 < D < 0.66$	up to 2	up to 2
$D > 0.66$	up to 3	up to 1

Output voltage control is achieved by applying the asymmetrical pulse width modulation (PWM) switching to each main and clamp switch pair. The three switch pairs are interleaved with 120° phase shift, which leads to an increased effective switching frequency resulting in smaller input-current ripple. The duty cycle of each main switch is in the whole range between 0 and 1. The ideal voltage ratio of the proposed converter can be expressed as

$$\frac{V_o}{V_i} = \frac{n}{1-D} \qquad (0 < D < 1) \tag{1}$$

where $n = N_S/N_P$. Also, the voltage across the clamp capacitor C_C can be obtained by

$$V_C = \frac{1}{1-D} \cdot V_i. \tag{2}$$

In order to simplify the analysis of the steady-state operation, several assumptions are made as follows.

1) Input inductance L_i is sufficiently large so that it can be considered as a constant current source.
2) Output capacitance C_o is sufficiently large so that it can be considered as a constant voltage source.
3) Dead time between main and clamp switch pair is ignored.
4) Magnetizing inductance is assumed to be infinite.
5) Total leakage inductances reflected to the primary of each phase are equal ($L_{\mathrm{k}1} = L_{\mathrm{k}2} = L_{\mathrm{k}3} = L_k$).

A. Principle of Operation

The proposed converter operates under three different regions according to the duty cycle: $D > 0.66$, $0.33 < D < 0.66$, and $D < 0.33$. The number of switches that simultaneously turn on is shown in Table I. The operating modes of the proposed converter are analyzed based on the three regions. In any case, the total number of switches that simultaneously turns on is 3.

1) Operation in D > 0.66: Fig. 2 shows key waveforms of the proposed converter in the case of $D > 0.66$. The converter has five operating modes within each third of an operating cycle, and the operation states of the five operating modes are shown in Fig. 3.

Mode I [t_0, t_1]: At time t_0, all the diode currents become zero, and therefore, the winding voltages become zero. Each of the

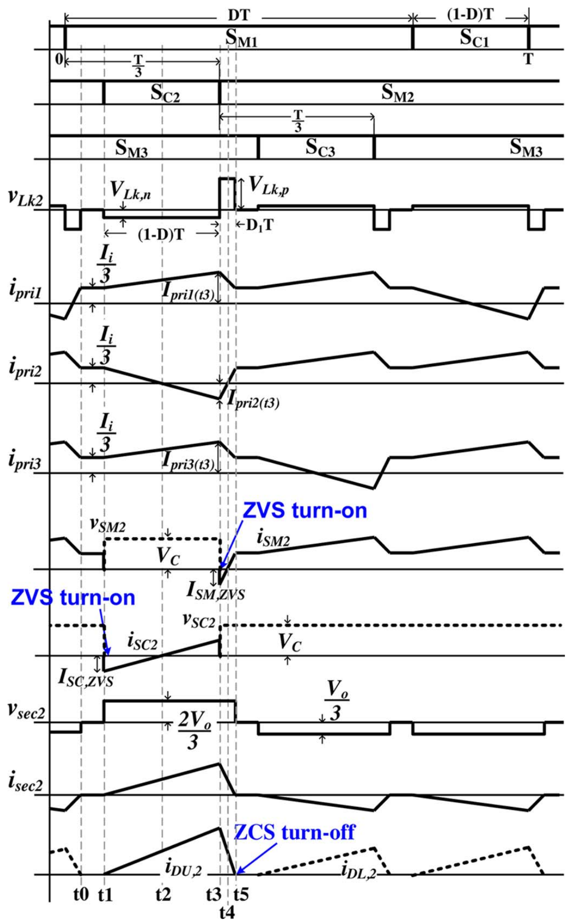

Fig. 2. Key waveforms of the proposed converter ($D > 0.66$).

primary winding current becomes identical:

$$i_{\mathrm{pri1}} = i_{\mathrm{pri2}} = i_{\mathrm{pri3}} = \frac{1}{3} I_i. \tag{3}$$

The output capacitor supplies the load during this mode.

Mode II [t_1, t_2]: At time t_1, main switch S_{M2} is turned off and the current i_{pri2} is commutated to the body diode of the clamp switch S_{C2}. This causes the current i_{pri2} to decrease and currents i_{pri1} and i_{pri3} to increase, leading to the conduction of the upper diode D_{U2} and lower diodes D_{L1} and D_{L3}, respectively, at the secondary. The voltages of the windings become

$$v_{\mathrm{pri2}} = \frac{1}{n} \cdot v_{\mathrm{sec2}} = \frac{1}{n} \cdot \frac{2}{3}\ V_o. \tag{4}$$

Then, the voltages across L_{k2} can then be obtained by

$$V_{\mathrm{Lk},n} = \frac{2}{3} \cdot \left(V_C - \frac{V_o}{n} \right). \tag{5}$$

The current i_{pri2} is decreasing with the slope determined by $V_{\mathrm{Lk},n}/L_k$. It is seen that the clamp switch S_{C2} is turned on with ZVS when the gate signal for S_{C2} is applied during this mode.

Mode III [t_2, t_3]: The current i_{pri2} reverses its direction of flow at t_2 and increases its magnitude while currents i_{pri1} and i_{pri3} keep increasing linearly. Since the average current through

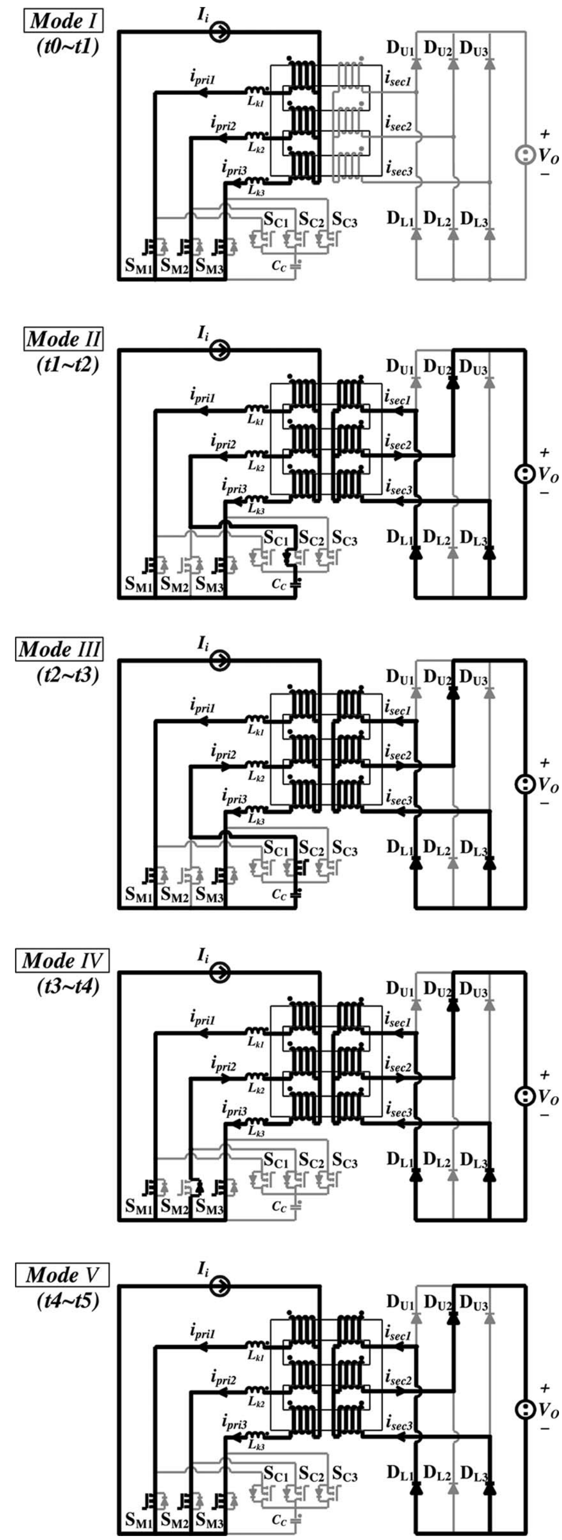

Fig. 3. Operation states of the proposed converter ($D > 0.66$).

each clamp switch is zero, $I_{\mathrm{pri2(t3)}}$ which is the magnitude of the current i_{pri2} at the end of Mode III can be obtained by

$$I_{\mathrm{pri2(t3)}} = -\frac{1}{3} I_i. \tag{6}$$

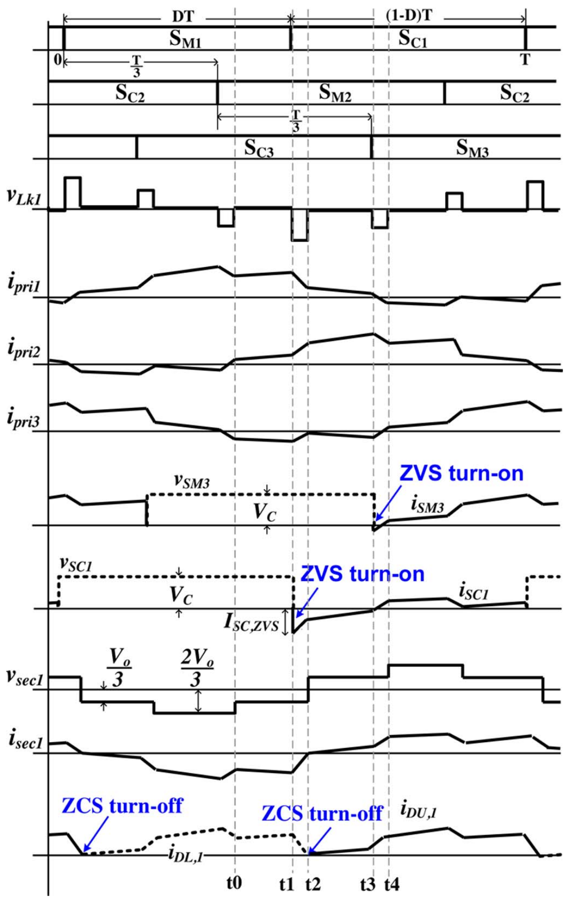

Fig. 4. Key waveforms of the proposed converter $(0.33 < D < 0.66)$.

Then, current magnitudes $I_{\mathrm{pri2(t3)}}$ and $I_{\mathrm{pri3(t3)}}$ at t_3 can be obtained by

$$I_{\mathrm{pri1(t3)}} = I_{\mathrm{pri3(t3)}} = \frac{2}{3} I_i. \tag{7}$$

Mode IV [t_3, t_4]: At time t_3, the clamp switch S_{C2} is turned off, and the current i_{pri2} is commutated to the body diode of the main switch S_{M2}. This causes all primary currents i_{pri1}, i_{pri2}, and i_{pri3} to decrease. The voltages across L_{k2} can then be obtained by

$$V_{\mathrm{Lk},p} = \frac{2V_o}{3n}. \tag{8}$$

The decreasing rate of the current i_{pri2} is determined by $V_{\mathrm{Lk},p}/L_k$. It should be noted that the main switch S_{M2} can be turned on with ZVS at this mode.

Mode V [t_4, t_5]: The current i_{pri2} reverses its direction of flow at time t_4 and increases its magnitude while currents i_{pri1} and i_{pri3} keep decreasing linearly until each of the primary winding current becomes identical, as shown in (1). It is also noted that the rectifier diodes D_{U2}, D_{L1}, and D_{L3} are turned off with ZCS. This is the end of one third of the cycle. The other parts of the cycle are repeated in the same fashion.

2) Operation in $0.33 < D < 0.66$: Fig. 4 shows key waveforms of the proposed converter in the case of $0.33 < D < 0.66$.

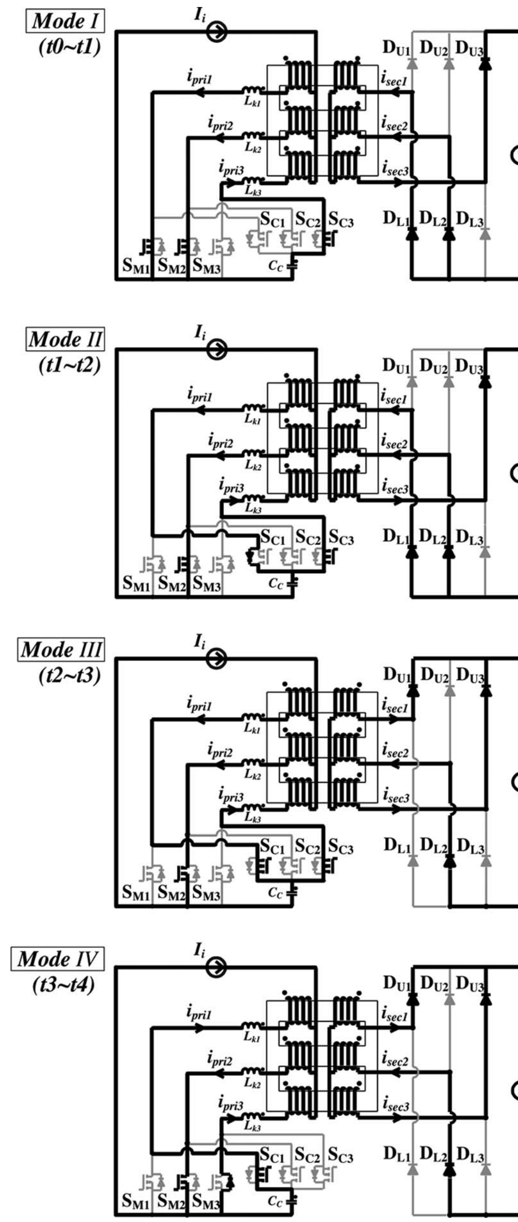

Fig. 5. Operation states of the proposed converter $(0.33 < D < 0.66)$.

The converter has four operating modes within each third of an operating cycle, and the operating states of each mode are shown in Fig. 5. At Mode I, two main switches S_{M1} and S_{M2} and one clamp switch S_{C3} are conducting. At time t_1, the main switch S_{M1} is turned off, and the current that was flowing through the main channel of S_{M1} is commutated to the body diode of S_{C1} as we can see in Mode II. When the gating signal is applied to S_{C1}, the current that was flowing through body diode of S_{C1} is commutated to its main channel, resulting in ZVS turn-on of S_{C1}. At time t_3, the clamp switch S_{C3} is turned off, and the current that was flowing through S_{C3} is commutated to the body diode of the main switch S_{M3} resulting in ZVS turn-on of S_{M3}. Both main switch S_{M1} clamp and switch S_{C3} are turned off with hard switching. Instead, all the switches are turned on with ZVS in this mode.

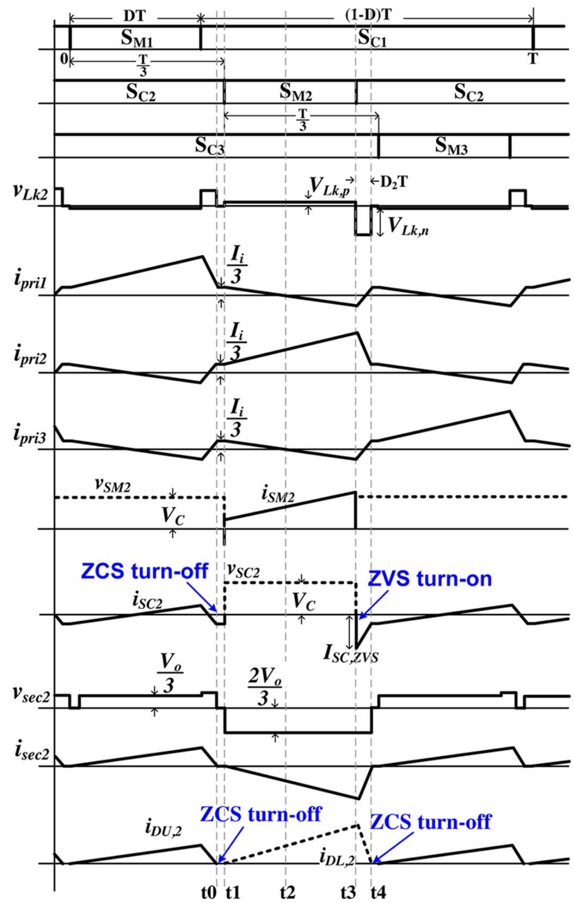

Fig. 6. Key waveforms of the proposed converter ($D < 0.33$).

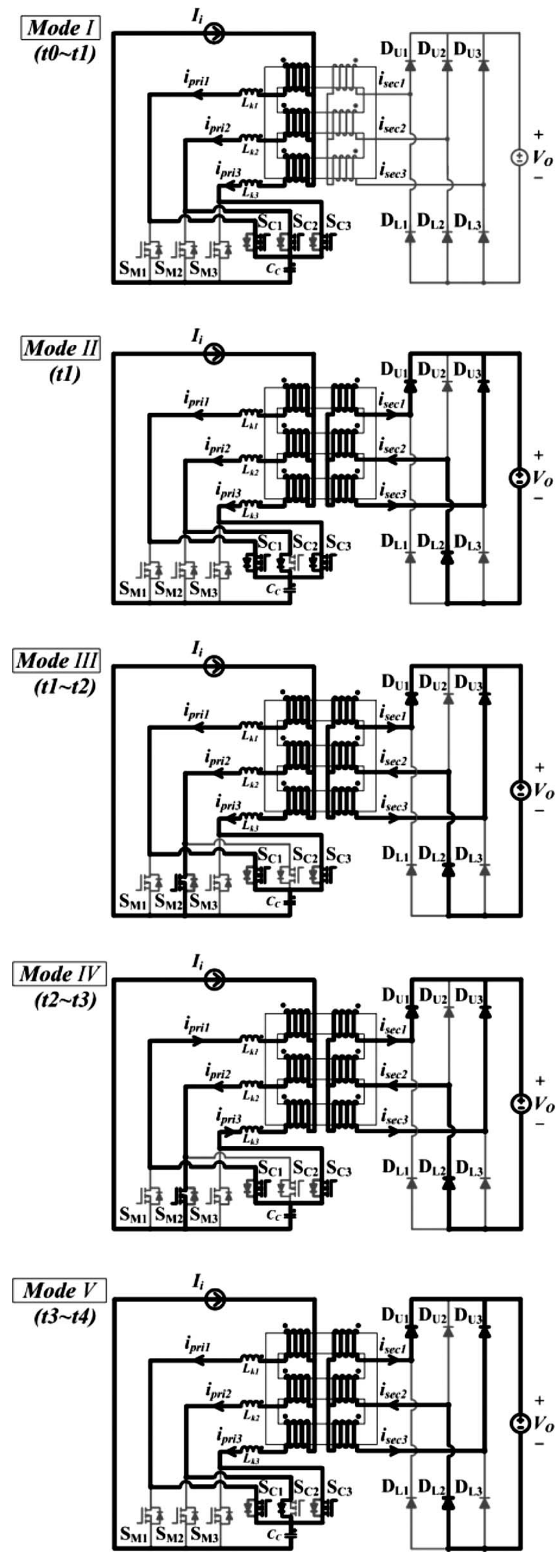

Fig. 7. Operation states of the proposed converter ($D < 0.33$).

3) Operation in $D < 0.33$: Fig. 6 shows key waveforms of the proposed converter in the case of $D < 0.33$. The converter has five operating modes within each third of an operating cycle, and the operating states of each mode are shown in Fig. 7.

At Mode I, all the main switches are being turned off, and all the clamp switches are conducting. At time t_1, the clamp switch $S_{\mathrm{C}2}$ is turned off, and the current that was flowing through main channel of $S_{\mathrm{C}2}$ is commutated to its body diode as we can see in Mode II. When the gating signal is applied to the main switch $S_{\mathrm{M}2}$, the current that was flowing through the body diode of $S_{\mathrm{C}2}$ is commutated to the main channel of the main switch $S_{\mathrm{M}2}$, resulting in hard switching of the main switch $S_{\mathrm{M}2}$. Instead, the clamp switch $S_{\mathrm{C}2}$ is turned off with ZCS.

Owing to the operation of clamp switches, the proposed converter can be operated with duty cycle less than 0.33, and therefore, no additional start-up circuit is necessary. In addition, this could improve dynamic characteristics of the closed-loop control system. Table II summarizes the soft switching condition for the proposed converter.

B. Voltage Conversion Ratio

The actual voltage conversion ratio of the proposed converter is derived for $D > 0.66$ case, considering the effect of voltage drop across the leakage inductor of the transformer. Applying the voltage-second balance principle to leakage inductor $L_{\mathrm{k}2}$ from Mode I to Mode V, the following equation can be obtained (see waveforms of $v_{\mathrm{Lk}2}$ and $i_{\mathrm{pri}2}$ in Fig. 2):

$$V_{\mathrm{Lk},n} \cdot (1 - D) \cdot T = V_{\mathrm{Lk},p} \cdot D_1 \cdot T. \qquad (9)$$

TABLE II
SUMMARY OF THE SOFT SWITCHING CONDITION

Duty cycle	Switching condition	Main Switches	Clamp Switches
D > 0.66 *0.33 < D < 0.66*	Turn On	ZVS	ZVS
	Turn Off	None	None
D < 0.33	Turn On	None	ZVS
	Turn Off	None	ZCS

From the waveforms of v_{Lk2} and i_{pri2}, it can be seen

$$\frac{V_{\mathrm{Lk},p}}{L_k} = \frac{1}{D_1 T}\left(\frac{1}{3}I_i - I_{\mathrm{pri2(t3)}}\right). \tag{10}$$

Using (2), (5), (6), and (8)–(10), the voltage conversion ratio for the $D > 0.66$ case can be obtained by

$$V_o = n\left(\frac{V_i}{(1-D)} - \frac{P_o \cdot L_k \cdot f_s}{V_i \cdot (1-D)\cdot \eta}\right) \tag{11}$$

where η is the converter efficiency, and $\eta \cdot I_i \cdot V_i = P_o$. In a similar way, the voltage conversion ratios for the $D < 0.33$ case can be derived. Applying the voltage-second balance principle to the leakage inductor L_{k2} (see waveforms of v_{Lk2} and i_{pri2} in Fig. 6), the following equation can be obtained:

$$V_{\mathrm{Lk},p} \cdot D \cdot T = V_{\mathrm{Lk},n} \cdot D_2 \cdot T. \tag{12}$$

From the waveforms of v_{Lk2} and i_{pri2} in Fig. 6, it can be seen

$$\frac{V_{\mathrm{Lk},n}}{L_k} = \frac{1}{D_2 T}\left(I_{\mathrm{pri2(t3)}} - \frac{1}{3}I_i\right). \tag{13}$$

Using (2), (12), and (13) and values $V_{\mathrm{Lk},n}$, $V_{\mathrm{Lk},p}$, and $I_{\mathrm{pri2(t3)}}$ obtained from Fig. 6, the voltage conversion ratio for $D < 0.33$ case can be obtained by

$$V_o = n\left(\frac{V_i}{1-D} - \frac{(1-D)\cdot P_o \cdot L_k \cdot f_s}{V_i \cdot D^2 \cdot \eta}\right). \tag{14}$$

The voltage conversion ratios for $0.33 < D < 0.66$ cases can be derived by, using (11) and (14),

$$V_o = n\left(\frac{V_i}{1-D} - \frac{2\cdot D \cdot P_o \cdot L_k \cdot f_s}{V_i \cdot (D-(2/9))\cdot \eta}\right). \tag{15}$$

From (11), (14), and (15), the actual voltage conversion ratio of the proposed converter is drawn in Fig. 8 as a function of the duty ratio *D* with different leakage inductances.

It is shown in Fig. 8 that at low duty cycle range the duty loss caused by leakage inductance of the transformer is significant, but as the duty cycle increases the effect of the leakage inductance is reduced. In fact, the higher the leakage inductance, switching frequency, and/or output power, the higher the duty loss.

C. ZVS Current and Range

As shown in Fig. 2, the ZVS current of the main switch $I_{\mathrm{SM,ZVS}}$ is the clamp switch current at turning off that is commutated to the main switch and used to discharge the output

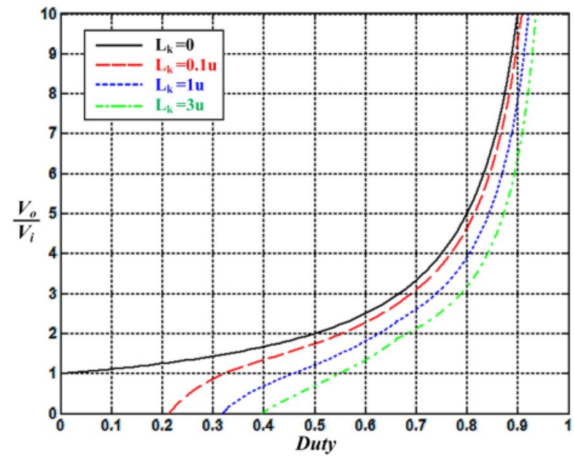

Fig. 8. Voltage conversion ratio as a function of duty cycle with different inductances (P_o = 5 kW, f_s = 50 kHz, N_S/N_P = 1, η = 0.95).

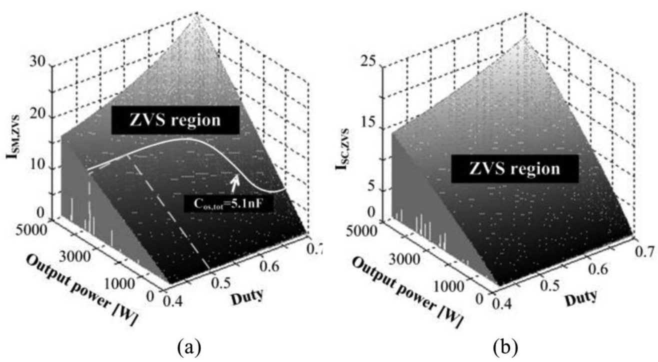

Fig. 9. ZVS current and ZVS region of switches: (a) main switch and (b) clamp switch.

capacitance of the main switch and is determined by

$$I_{\mathrm{SM,ZVS}} = I_{\mathrm{pri2(t3)}} = \frac{1}{3}I_i. \tag{16}$$

To ensure the ZVS turn-on of the main switch, the following condition should be satisfied:

$$\frac{1}{2}\cdot L_k \cdot I_{\mathrm{SM,ZVS}}^2 > \frac{1}{2}\left(C_{\mathrm{os},M} + C_{\mathrm{os},C}\right)\cdot V_C^2 \tag{17}$$

where $C_{\mathrm{os},M}$ and $C_{\mathrm{os},C}$ are the output capacitances of the main switch and clamp switch, respectively.

The ZVS current of the clamp switch $I_{\mathrm{SC,ZVS}}$ is the main switch current at turning off that is commutated to the clamp switch and used to discharge the output capacitance of the clamp switch and is determined by

$$I_{\mathrm{SC,ZVS}} = \frac{1}{3}I_i. \tag{18}$$

To ensure the ZVS turn-on of clamp switch S_{C2}, the following condition should be satisfied:

$$\frac{1}{2}\cdot L_k \cdot I_{\mathrm{SM,ZVS}}^2 > \frac{1}{2}\left(C_{\mathrm{os},M} + C_{\mathrm{os},C}\right)\cdot V_C^2. \tag{19}$$

Using (16)–(19), the ZVS currents and ZVS ranges of main and clamp switches as the function of duty cycle and output power are plotted, respectively, as shown in Fig. 9. As shown in

TABLE III

COMPARISON OF CHARACTERISTICS OF THE PROPOSED AND CONVENTIONAL CONVERTERS ($P_o = 5$ kW, $V_i = 60$–110 V, $V_o = 380$ V, $f_s = 50$ kHz, $L_k = 1.1\ \mu$H)

		Proposed Converter	PCPP Converter[14]	Half-bridge Converter[12]	V6 Converter[7]
Topology		3-phase Current-fed	3-phase Current-fed	3-phase Current-fed	3 single phase Voltage-fed
Clamping method		Active clamping	Passive clamping	Active clamping	Passive clamping
Switching method		Soft switching	Hard switching	Soft switching	Soft switching
Duty cycle range (Operating duty cycle)		0<D<1 (0.42<D<0.71)	0.33<D<1 (0.37<D<0.7)	0<D<1 (0.43<D<0.7)	0<D<0.33 (0.07<D<0.32)
Start up circuit		None	Required	None	None
Additional clamp or snubber		Not required	Required at the primary	Not required	Required at the secondary
Diode Reverse recovery loss		Negligible	Not negligible	Negligible	Not negligible
Input filter		Not required	Not required	Not required	Required
Circuit complexity		Relatively complicated	Simple	Relatively Complicated	Most complicated
switches	Main	200V, 34A, 3EA	250V, 37A, 3EA	200V, 38A, 3EA	110V, 29A, 12EA
	Clamp	200V, 9A, 3EA	-	200V, 18A, 3EA	-
	Switch utilization	0.112	0.138	0.065	0.066
Diodes		380V, 4.4A, 6EA	380V, 4.4A, 6EA	380V, 4.4A, 6EA	414V, 4.4A, 6EA
Transformer	Turn ratio	1 : 2	1 : 2	1 : 2	1 : 4
	KVA rating	7.7kVA	7.4kVA	10.8kVA	5.3kVA

Fig. 9(a), the ZVS current of the main switch tends to increase as the output power increases and/or as the duty cycle increases. This means that the ZVS turn-on of the main switch can be more easily achieved under the condition of higher output power and duty cycle. It is noted that the ZVS range of the main switch becomes broader for smaller total output capacitance $C_{\mathrm{os,tot}} = C_{\mathrm{os},M} + C_{\mathrm{os},C}$ of MOSFETs. For example, if MOSFETs with total output capacitance $C_{\mathrm{os,tot}}$ of 5.1 nF are selected in this example, the ZVS turn-on of the main switch can be achieved with output power which is greater than 3800 W at duty cycle of 0.5 [see Fig. 9(a)]. The ZVS current of the clamp switch tends to increase as the output power decreases and duty cycle increases. It should be noted from Fig. 9(b) that the ZVS turn-on of the clamp switch can be achieved in the overall duty cycle and output power ranges.

D. Comparative Analysis

In this section, main characteristics and device ratings of the proposed converter are compared to the conventional converters including two three-phase current-fed converters (the passive-clamped push–pull converter (PCPP converter) [14] and the L-type half-bridge converter [12]) and a three-phase voltage-fed converter (V6 converter) [7]. The comparison results are summarized in Table III. Owing to the active clamping, the duty cycle of the proposed converter and the L-type half-bridge converter ranges from 0 to 1, which may result in better dynamic response in transient state. The current-fed push–pull converter requires an additional start-up circuit at the primary since the duty cycle less than 0.33 is not allowed without it. A clamp or snubber may be required for the V6 converter to suppress the voltage spike and ringing that is generated between transformer leakage inductance and diode junction capacitance at the secondary. The losses associated with the passive clamp circuit in the PCPP converter [14] are more significant. The proposed converter and the half-bridge converter [12] do not require start-up and clamp circuits. The input current ripple of all the current-fed converters is much smaller than that of the voltage-fed converter [7] in which an input filter is required. The PCPP converter [14] has the smallest number of switches while the V6 converter [7] has the largest number of switches. Even if the number of switch of the proposed converter is twice that of the PCPP converter [14], the switch utilization ratios of the both converters are similar and much higher than those of the half-bridge [12] and V6 converters. The V6 converter has the lowest kVA rating of the transformer. The kVA rating of the transformer of the proposed converter is 30% smaller than that of the half-bridge converter. The losses associated with diode reverse recovery of the proposed converter are negligible since diodes are turned off with ZCS unlike the PCPP [14] and V6 converters. In summary, the features of the proposed converter such as soft switching of both main and clamp switches, lossless clamping at the primary, and negligible losses associated with diode reverse recovery result in an improvement of overall efficiency and power density.

E. Design Example

In this section, a design example of the proposed converter as a front-end dc–dc converter for fuel cell application is presented, considering the following system parameters:

$$P_o = 5\text{ kW},\ V_i = 60\text{–}110\text{ V},\ V_o = 380\text{ V},\ f_s = 50\text{ kHz},$$
$$L_k = 1.1\ \mu\text{H}.$$

Then, the average value of the rated input current I_i $(=P_o/V_i)$ becomes 83.3 A. Since the converter is operated with maximum duty cycle at rated load for fuel cell application, it is preferred that the maximum duty to be greater than 0.66. Therefore, using (11), the operating range of the duty cycle can be calculated as, when $n = 2$,

$$0.42 < D < 0.71 \tag{20}$$

where efficiency of 95% is assumed. Duty cycle D_1 is calculated to be 0.02 using (10).

1) *Switches:* Since the voltage rating of both main and clamp switches is the same as the voltage across clamp C_c, it is calculated by

$$\frac{V_{i,\min}}{1 - D_{\max}} = 206.9\ \text{V}. \tag{21}$$

From Fig. 2, the current ratings of the main and clamp switches in rms value can be calculated to be 34.4 and 8.7 A, respectively.

2) *Diodes:* The voltage rating of rectifier diodes is the same as the output voltage which is 380 V. It can be seen from Fig. 1 that the average values of upper and lower diode currents are the same and can be obtained by

$$I_{\text{DU,avg}} = I_{\text{DL,avg}} = (1 - D + D_1) \cdot \frac{I_i}{6} = 4.33\ \text{A}. \tag{22}$$

3) *Transformer:* In this example, an off-the-shelf EI core of the ferrite material ($B_{\text{sat}} = 0.3$ T, $\mu_i = 2500$) is used for the three-phase transformer. The required area product of the core can be obtained by

$$A_P = \frac{2\, V_{\text{pri}} \cdot I_{\text{pri,rms}} \cdot (1 - D + D_1)}{B_m \cdot J \cdot K_f \cdot f_s} = 45.1\ \text{cm}^4 \tag{23}$$

where maximum flux density $B_{\max} = 0.7 B_{\text{sat}}$ T, current density $J = 3$ A/mm^2, and winding fill factor $k_f = 0.2$. Considering some margins, an EI core with $A_P = 203$ cm^4 has been chosen from a manufacture, as shown in Fig. 10. The parameters of the chosen core are as follows:

a) core window area: $W_a = 16.56$ cm^2;
b) core cross-sectional area: $A_c = 12.27$ cm^2.
Since the cross-sectional area of the center leg of the core is twice them of the both side legs, the center leg is cut out so as to have equal width, as shown in Fig. 10. Then, the parameter of the modified core is changed as follows:
c) core window area: $W_a = 22.6$ cm^2;
d) core cross sectional area: $A_c = 8.5$ cm^2.

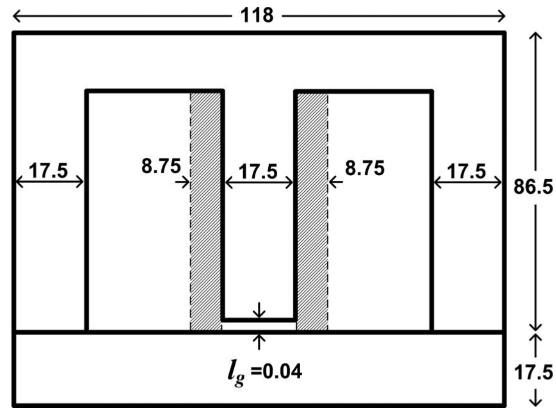

Fig. 10. Dimension of the three-phase core (mm).

From the modified core of Fig. 10, range of the number of primary winding turns can be obtained by

$$\frac{V_{\text{pri}}}{A_c} \cdot \frac{1 - D + D_1}{2B_m \cdot f_s} < N_P < \frac{1}{4} \cdot \frac{W_a \cdot J \cdot K_f}{I_{\text{pri,rms}}}. \tag{24}$$

That is, $2.22 < N_p < 11.94$. Then, the desired number of primary turns is chosen to be 11 so that current through magnetizing inductance is minimized. Even though widths of all three legs are equal, magnetizing inductance of the center leg is still larger than them of the both side legs since magnetic path length of the center leg is longer than them of the both side legs. This may cause more than 20% of unbalance in magnetizing inductances of the three legs [16]. In order to decrease the unbalance in magnetizing inductances, a small air gap of 0.04 mm was added at the center leg of the transformer.

III. Experimental Results

In order to verify the effectiveness of the proposed converter, 5-kW laboratory prototypes of both the PCPP converter [14] and the proposed active-clamped converter have been constructed, and the experimental results along with loss analysis are presented in this section. The system specifications used in the experiment are the same as ones used in Section II-D. Same switches, diodes, and transformers except clamping circuit have been used for prototypes of both converters. The residual-current device (RCD) clamp circuit ($R = 300\ \Omega$, $C = 9\ \mu$F, FRD 600 V 30 A) was employed for the PCPP converter. The implemented circuit diagram of the proposed converter is shown in Fig. 11. Switching devices were selected from the manufactures according to the component ratings calculated in Section II-E. The transformer was built using the core in Fig. 10 as well. The measured magnetizing inductances of each phase of the transformer are 690, 701, and 716 μH, respectively, which means less than 3% of unbalance.

The proposed converter is considered as a front-end dc–dc converter for fuel cell application. All experimental waveforms and loss analysis in this section are obtained from a programmable power source that emulates a fuel cell *V–I* characteristic (60 V at full load and 110 V at no load). Experimental

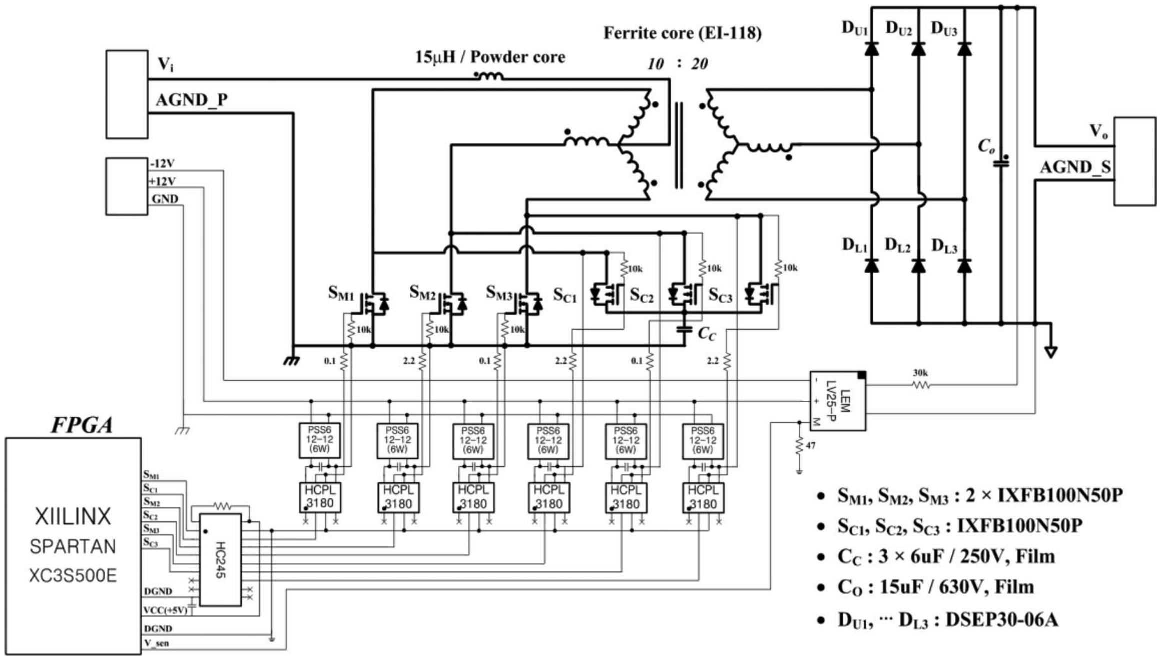

Fig. 11. Schematic of the implemented circuit.

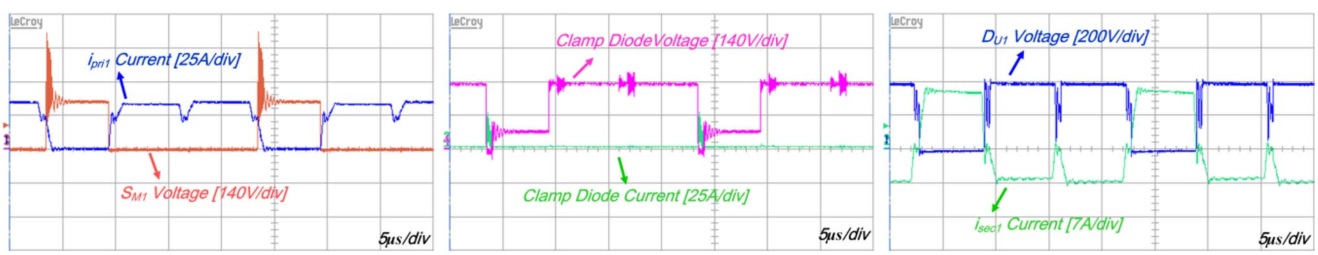

(a) (b) (c)

Fig. 12. Experimental waveforms of the PCPP converter [14] at $P_o = 5$ kW ($D = 0.7$). (a) Main switch. (b) Clamp diode. (c) Rectifier diode.

waveforms obtained from the PCPP converter [14] at full load are provide in Fig. 12. It is seen that the voltage surge and ringing across the main switch are significant, which results in increased turn-on switching losses of main switches. The voltage surge can be reduced by reducing a resistance value in RCD snubber, but this will in turn increase the loss in the resistor. Note that the volume of the resistor in the RCD snubber is considerable since approximately 317 W is consumed in the resistor at full load. Experimental waveforms of the proposed converter at two different operating duty cycles $D = 0.71$ ($V_i = 60$ V) and $D = 0.6$ ($V_i = 80$ V) are shown in Figs. 13 and 14, respectively. Fig. 13(a) shows the full-load input current and three primary transformer currents of the proposed converter. It can be seen that the input current ripple has been greatly reduced due to the interleaving effect. It should also be noted from Fig. 13(a) that three transformer primary currents have less than 5% of unbalance in their rms values. It is seen from Fig. 13(b) and (c) that both the main and clamp switches are being turned on with ZVS. Fig. 13(d) shows that the rectifier diode is turned off with ZCS. The ZVS turn-on of the main switch of the proposed converter for this fuel cell application is achieved only for the duty cycle range $D > 0.66$ ($P_o > 4$ kW or $V_i < 70$ V). Therefore, the main switch is hard switched at 3.2 kW ($D = 0.6$), as shown in Fig. 15(a). This is not a problem in the fuel cell application where full-load efficiency should be optimized since the system is operated at full load during most of time. If this is not for fuel cell application, and therefore, more power could be drawn at duty cycle range $0.33 < D < 0.66$ so that $I_{\mathrm{SM,ZVS}}$ is sufficient to satisfy (17), the main switch could be turned on with ZVS, as shown in Fig. 4.

The measured using Yokogawa's power analyzer WT3000 and calculated efficiencies of both proposed and PCPP converters are shown in Fig. 15. Efficiency improvement of the proposed converter is mostly resulting from reduced losses associated with clamp circuit. The peak measured efficiency of the proposed converter is 97.1% at 2 kW and the measured full-load efficiency is 94.6% at 5 kW. The peak measured efficiency of the PCPP converter is 91.8% at 2.3 kW and the measured full-load efficiency is 88.1% at 5 kW.

Fig. 16 shows a calculated loss comparison of the proposed and PCPP converters at full load. In the PCPP converter, the losses associated with the RCD clamp circuit are considered as a major part of the total converter power loss, and at full load the loss occupies larger than 50% of the total power loss. The

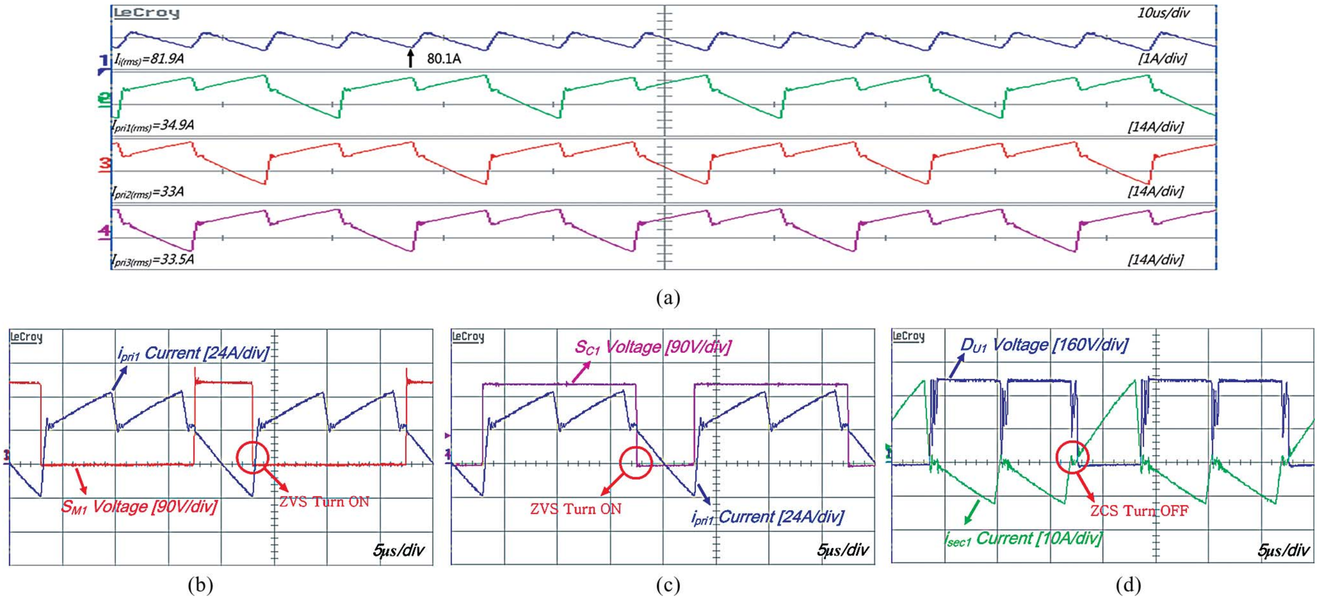

Fig. 13. Experimental waveforms of the proposed converter at $P_o = 5$ kW ($D = 0.71$). (a) Input and the primary winding current. (b) Main switch. (c) Clamp switch. (d) Rectifier diode.

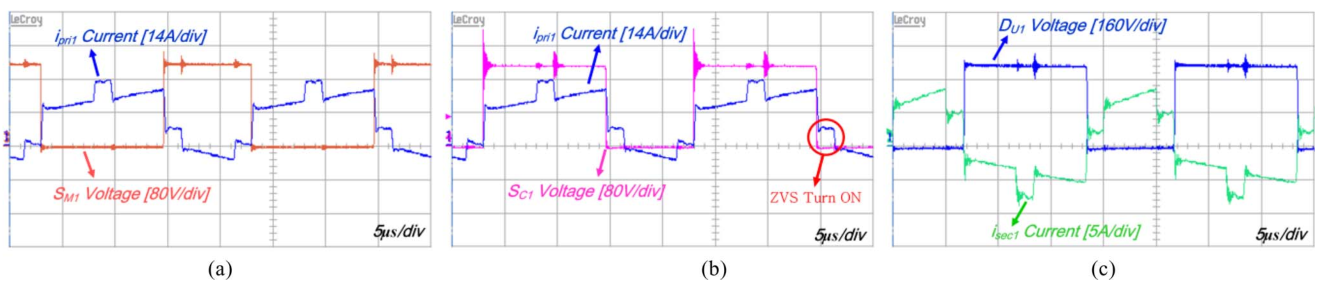

Fig. 14. Experimental waveforms of the proposed converter at $P_o = 3.2$ kW ($D = 0.6$). (a) Main switch. (b) Clamp diode. (c) Rectifier diode.

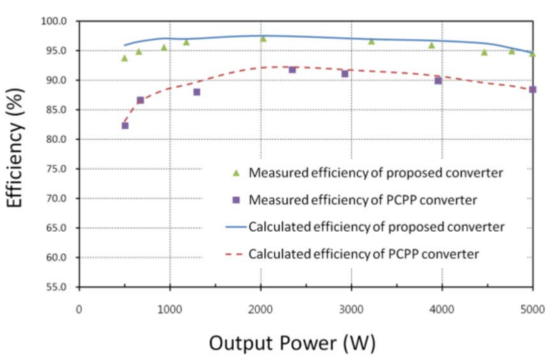

Fig. 15. Efficiency of the proposed and PCPP converters.

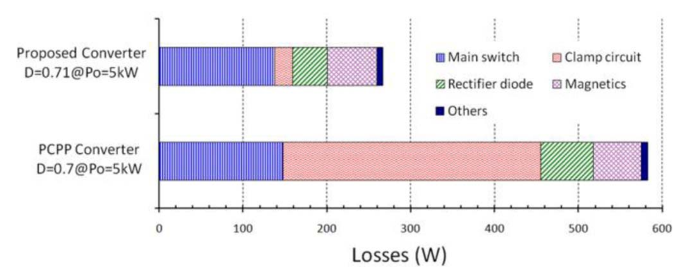

Fig. 16. Loss comparison of the proposed and PCPP converters at full load.

losses associated with clamp circuit of the proposed converter are greatly reduced since resistive loss in the active-clamp circuit is negligible, and the clamp switch is turned on with ZVS, resulting in significant improvement of efficiency at full load. Also, rectifier diode loss of the proposed converter is mostly diode conduction loss since the diode is turned off with ZCS whereas the rectifier diode of the PCPP converter has the diode conduction loss as well as turn-off losses associated with diode reverse recovery. The two converters have little difference in magnetic loss. Fig. 17 shows comparison of loss distribution according to three different operating modes (or load power) of the proposed converter. As the load increases, the conduction losses of main switches are sharply increased and the portion in the total converter power loss is also increased. At full load of 5 kW, the losses associated with main switches occupy 53% (46% of conduction loss and 7% of turn-off loss) of the total power loss, as shown in Fig. 17 (a). Since the proposed converter was optimized at full load for fuel cell applications, the leakage inductance was minimized in the design, and therefore, ZVS of main switches are not achieved for $0.33 < D < 0.66$.

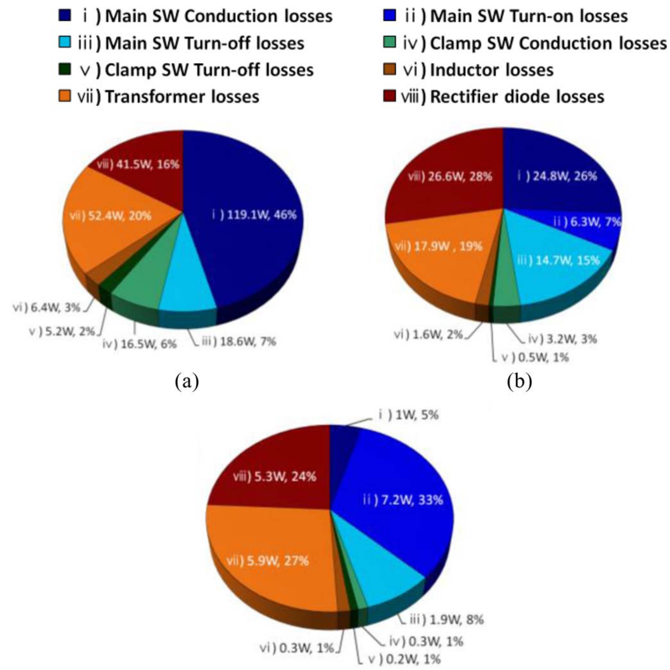

Fig. 17. Power loss distribution of the proposed converter for (a) full load ($D = 0.71$, $P_o = 5$ kW), (b) medium load ($D = 0.6$, $P_o = 3.2$ kW, and (c) light load ($D = 0.5$, $P_o = 500$ W).

Fig. 18. Photograph of the proposed converter.

However, if the converter is not for fuel cell application and thus full load may occur at any duty cycle, the proposed converter could be designed to achieve ZVS turn-on of main switches for $0.33 < D < 0.66$. Even though the main switch in this application is hard switched for $D = 0.6$ ($P_o = 3.2$ kW), as shown in Fig. 14(a), turn-on loss of main switches is only 7% of the total power loss, as shown in Fig. 17(b) since most of the loss still come from conduction losses of main switches and diodes. The transformer loss occupies 19–27% of the total power loss for all cases, and the difference in absolute loss value is the copper loss since the core loss does not change much according to load variation. As the load decreases, the turn-on loss of main switches is sharply increased and the portion in the total power loss is also increased. At light load of 500 W, the most dominant loss is the switching losses of main switches including turn-on loss that occupies 33% of the total power loss whereas the conduction loss of main switches is negligible. Fig. 18 shows the photograph of the 5-kW prototype of the proposed converter.

IV. Conclusion

A new three-phase current-fed push–pull dc–dc converter with active clamping is proposed in this paper. The proposed converter features active clamping of the transient surge voltage, natural ZVS turn-on of main switches and clamp switches, full operating duty cycle range between 0 and 1, and ZCS turn-off of rectifier diodes. Comparative evaluation shows effectiveness of the proposed converter in overall performances. Experimental results from 5-kW laboratory prototypes of the proposed and PCPP converters demonstrate that the proposed converter could be a viable solution for high-power application such as fuel cells in that high efficiency and high power density can be achieved.

References

[1] X. Kong, L. T. Choi, and A. M. Khambadkone, "Analysis and control of isolated current-fed full bridge converter in fuel cell system," in *Proc. IEEE Ind. Electron. Conf. (IECON)*, Nov. 2004, vol. 3, pp. 2825–2830.

[2] V. Yakushev, V. Meleshin, and S. Fraidlin, "Full-bridge isolated current fed converter with active clamp," in *Proc. IEEE Appl. Power Electron. Conf. (APEC'99)*, Mar., vol. 1, pp. 560–566.

[3] A. R. Prasad, P. D. Ziogas, and S. Manias, "Analysis and design of a three-phase offline DC–DC converter with high-frequency isolation," *IEEE Trans. Ind. Appl.*, vol. 28, no. 4, pp. 824–832, Jul./Aug. 1992.

[4] D. de Souza Oliveira, Jr. and I. Barbi, "A three-phase ZVS PWM dc/dc converter with asymmetrical duty cycle for high power applications," *IEEE Trans. Power Electron.*, vol. 20, no. 2, pp. 370–377, Mar. 2005.

[5] D. de S. O. Jr. and I. Barbi, "A three-phase ZVS PWM dc–dc converter with asymmetrical duty cycle associated with a three-phase version of the hybridge rectifier," *IEEE Trans. Power Electron.*, vol. 20, no. 2, pp. 354–360, Mar. 2005.

[6] H. Kim, C. Yoon, and S. Choi, "A three-phase zero-voltage and zero-current switching dc–dc converter for fuel cell applications," *IEEE Trans. Power Electron.*, vol. 25, no. 2, pp. 391–398, Feb. 2010.

[7] C. Liu, A. Johnson, and J. Lai, "A novel three-phase high-power soft-switched dc–dc converter for low-voltage fuel cell applications," *IEEE Trans. Ind. Appl.*, vol. 41, no. 6, pp. 1691–1697, Nov./Dec. 2005.

[8] M. Mohr and F. W. Fuchs, "Current-fed full bridge converters for fuel cell systems connected to the three phase grid," in *IEEE Ind. Electron. Conf. (IECON)*, 2006, pp. 4313–4318.

[9] H. Kim, C. Yoon, and S. Choi, "An improved current-fed ZVS isolated boost converter for fuel cell applications," in *IEEE Appl. Power Electron. Conf. (APEC)*, 2008, pp. 593–599.

[10] H. Cha, J. Choi, and P. Enjeti, "A three-phase current-fed dc–dc converter with active clamp for low-dc renewable energy sources," *IEEE Trans. Power Electron.*, vol. 23, no. 6, pp. 2784–2793, Nov. 2008.

[11] S. V. G. Oliveira, C. E. Marcussi, and I. Barbi, "An average current-mode controlled three-phase step-up dc–dc converter with a three-phase high frequency transformer," in *Proc. IEEE Power Electron. Spec. Conf. (PESC)*, Jun. 2005, pp. 2623–2629.

[12] H. Cha, J. Choi, and B. Han, "A new three-phase interleaved isolated boost converter with active clamp for fuel cells," in *Proc. IEEE Power Electron. Spec. Conf. (PESC)*, Jun. 2008, pp. 1271–1276.

[13] C. Yoon and S. Choi, "A multi-phase dc–dc converters using a boost half bridge cell for high voltage and high power applications," in *Proc. IEEE Int. Power Electron. Motion Control Conf. (IPEMC)*, May 2009, pp. 780–786.

[14] R. L. Andersen and I. Barbi, "A three-phase current-fed push–pull dc–dc converter," *IEEE Trans. Power Electron.*, vol. 24, no. 2, pp. 358–368, Feb. 2009.

[15] M. H. Kheraluwala, D. W. Novotny, and D. M. Divan, "Design considerations for high power high frequency transformers," in *IEEE Power Electron. Spec. Conf. (PESC)*, 1990, pp. 734–742.

[16] J. A.-G. and G. Moon, "High-power-density three-phase converter utilizing a balanced-flux transformer core," in *IEEE Energy Conv. Congr. Expo. (ECCE)*, 2009, pp. 1039–1045.

[17] G. Franceschini, E. Lorenzani, M. Cavatorta, and A. Bellini, “3boost: A high-power three-phase step-up full-bridge converter for automotive applications,” *IEEE Trans. Ind. Electron.*, vol. 55, no. 1, pp. 173–183, Jan. 2008.

[18] S. Lee and S. Choi, “A three-phase current-fed push–pull dc–dc converter with active clamp for fuel cell applications,” in *Proc. IEEE Appl. Power Electron. Conf. (APEC)*, Feb., 2010, pp. 1934–1941.

Sangwon Lee was born in Seoul, Korea, in 1983. He received the B.S. and M.S. degrees from the Department of Control and Instrumentation Engineering, Seoul National University of Science and Technology, Seoul, Korea, in 2008 and 2010, respectively.

He is currently an Engineer at the Research and Development Center, Changsung, Inc., Incheon, Korea. His research interests include high-power dc–dc converter for new and renewable energy.

Junsung Park received the B.S. and M.S. degrees from the Seoul National University of Science and Technology (Seoul Tech), Seoul, Korea, in 2009 and 2011, respectively. He is currently working toward the Ph.D. degree at the Power Electronics and Fuel Cell Power Conditioning Laboratory, Seoul Tech.

His research interests include high power dc–dc converter for electric vehicles and renewable energy systems.

Sewan Choi (S’92–M’96–SM’04) received the B.S. degree in electronic engineering from Inha University, Incheon, Korea, in 1985, and the M.S. and Ph.D. degrees in electrical engineering from Texas A&M University, College Station, in 1992 and 1995, respectively.

From 1985 to 1990, he was with Daewoo Heavy Industries as a Research Engineer. From 1996 to 1997, he was a Principal Research Engineer at Samsung Electro-Mechanics Company, Korea. In 1997, he joined the Department of Control and Instrumentation Engineering, Seoul National University of Science and Technology (Seoul Tech), Seoul, Korea, where he is currently a Professor. His research interests include three-phase power factor correction, power conversion technologies in renewable energy systems, and dc–dc converters for hybrid electric and fuel cell vehicles.

Dr. Choi directed a student team to design and build a 10-kW fuel cell inverter for residential applications, which won the first place award in the 2003 Future Energy Challenge Competition sponsored by the US Department of Energy. He is an Associate Editor of the IEEE TRANSACTIONS ON POWER ELECTRONICS and IEEE TRANSACTIONS ON INDUSTRY APPLICATIONS.